Research Article | Vol. 27, No. 10 | 13 May 2019 | OPTICS EXPRESS 14577

Optics EXPRESS

Gate tunable graphene-integrated metasurface modulator for mid-infrared beam steering

C. SHI,* I. J. LUXMOORE, AND G. R. NASH

College of Engineering Mathematics and Physics, University of Exeter, EX4 4QF, Exeter, United Kingdom
**cs595@exeter.ac.uk*

Abstract: The ability to integrate graphene into metasurface devices has attracted enormous interest as a means of achieving dynamic electrical control of their electromagnetic response. In this manuscript, we experimentally demonstrate a graphene-integrated metasurface modulator that establishes the potential to actively control the amplitude and phase of mid-infrared light with high modulation depth and speed, in good agreement with simulation results. Our simulations also show it is possible to construct a reconfigurable surface with tunable phase profile by incorporating graphene-integrated metasurface modulators with specific geometric parameters. This reconfigurable surface is able to manipulate the orientation of the wave reflected from it, achieving a high-speed, switchable beam steering reflective interface. The results here could inspire research on dynamic reflective display and holograms.

Published by The Optical Society under the terms of the Creative Commons Attribution 4.0 License. Further distribution of this work must maintain attribution to the author(s) and the published article's title, journal citation, and DOI.

1. Introduction

Metasurfaces, planar metamaterials with a subwavelength thickness, enable the design of innovative, compact electromagnetic wave components with multiple functionalities due to the extraordinary values of permittivity or permeability that can be achieved [1–4]. Although it has been shown that metasurfaces are able to control and manipulate electromagnetic propagation from the microwave to the visible by altering its amplitude, phase [5–7], and polarization states [8,9] in a desired manner, the lack of sufficient tunability limits their applications. Intensive efforts have been made to dynamically control the response of metasurface based modulators [10–17] for applications such as high data rate communication [10,11], reconfigurable surfaces [12,13], and imaging [14]. As a result, solid state modulators based on varactors [12] or PIN diodes [15] are now quite versatile at radio frequencies, and fast and highly tunable terahertz modulators can also be realized using metasurfaces with compound semiconductors [10]. However, the mid-infrared range remains challenging due to the limited choice of materials. Modulators based on electrically controlled liquid crystal (LC) [16] or thermal controlled vanadium dioxide (VO_2) [17] suffer from slow modulation speed, while others based on semiconductor quantum wells require precise control on material growth and temperature [18]. Recent work has also investigated devices based on a combination of a MEMS (micro-electro-mechanical-system) platform and metasurface to steer mid-infrared light [19], but such devices require sophisticated integration techniques to realise.

Thanks to its unique gapless band structure, graphene has a highly tunable electrical conductivity that can be modulated within the order of nanoseconds, far quicker than conventional LC and VO_2 modulators, via electrostatic gating, or optical excitation [20–22]. Although the integration of graphene into metasurface devices is a promising approach for designing active mid-infrared modulators, up to now most research has focused on theoretical investigations [23–28].

#361993 https://doi.org/10.1364/OE.27.014577
Journal © 2019 Received 11 Mar 2019; revised 24 Apr 2019; accepted 30 Apr 2019; published 6 May 2019

Optics EXPRESS

In this paper, we present the experimental demonstration of a high-speed, compact graphene metasurface mid-infrared modulator, which allows a wide range of phase modulations by tuning the Fermi energy (E_F) of graphene via an applied gate voltage. Furthermore, a prototype mid-infrared reconfigurable surface is proposed to function as a beam steering lens that has the potential to switch from specular reflection to anomalous reflection at very high rates.

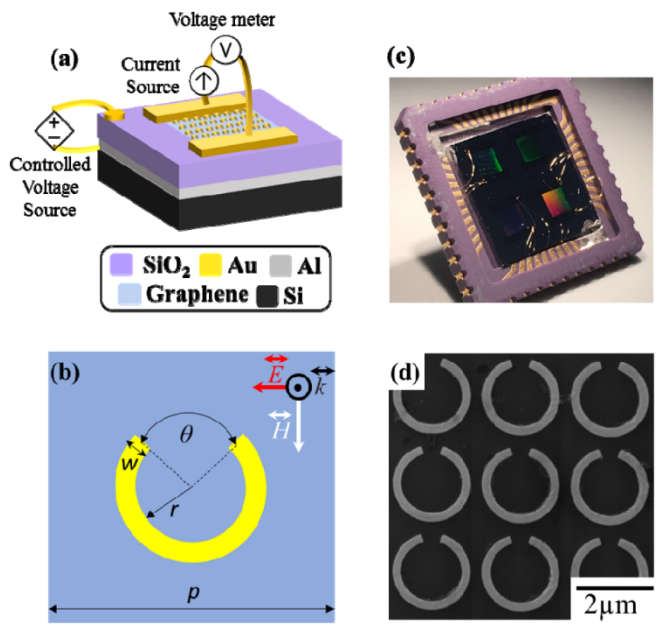

Fig. 1. Schematic of the graphene metasurface modulator (a) 3D view, (b) top view (c) Optical Photo of the fabricated device (d) SEM photo of the metasurface structure

2. Device fabrication and measurement

Our sample is composed of a monolayer graphene and split ring resonators (SRRs) metasurface, as schematically shown in Fig. 1. A highly doped Si-substrate was used, onto which a 50nm-thick aluminium conductive layer followed by a 300nm-thick silicon dioxide (SiO_2) spacer layer were deposited. Monolayer chemical vapor deposition (CVD) graphene was then transferred onto the sample and etched into a 2cm × 2cm square by the combination of oxygen and argon plasma. An array of periodic split ring resonators, together with electrical contacts, were patterned by electron beam lithography (EBL) and metalized by chromium and gold via thermal evaporation. The sample was mounted and wire bonded to a ceramic chip carrier for characterization.

Figure 1(d) shows a scanning electron microscope (SEM) image of a device with the inner radius of the ring r = 900nm, ring width w = 200nm, angular split gap θ = 32° and periodicity p = 2.8μm. The whole design is equivalent to a metasurface Salisbury screen with graphene integrated into it. The Salisbury screen, which has been widely used as absorbent device for radar detection, is an asymmetric Fabry-Perot resonance cavity that can eliminate reflection and achieve total absorption. The metasurface patterned on the Salisbury screen can also be regarded as a RLC circuit, which introduces a wavelength-dependent impedance to the device. When this effective impedance fulfills the impedance matching condition, reflection at this wavelength will be eliminated. Integration of graphene allows the wavelength at which reflection cancels out to be varied by modulation of the graphene conductivity.

All measurements were then performed at room temperature under ambient conditions. Field effect characteristic of devices with and without the ring resonators were first measured

Optics EXPRESS

by the setup schematically shown in the yellow shaded region of Fig. 2(a) and the results are plotted in Fig. 2(b). In both cases, the measured resistance has a maximum when the gate voltage, $V_g \approx 60$ V corresponding to the charge neutral point (CNP). The large positive value of V_{CNP} is consistent with the CVD graphene used in our sample having a significant intrinsic hole doping, as observed previously [29,30]. In addition, the very similar field characteristic obtained indicate that the ring resonators do not significantly affect the electrical characteristics of the graphene. The reflectivity of the devices was measured using a confocal system consisting of a 40x reflecting objective lens, which was mounted on a xy-stage so that it could be scanned over the surface, coupled to a FTIR spectrometer (Fig. 2(a)) [31]. The device was orientated such that the linearly polarized light from the FTIR source is parallel to the gap of the SRRs as shown in Fig. 1(b). Figure 2(c) shows the spatial variation of the measured reflectance integrated from 2.5 µm to 12.5 µm. The area with the smallest overall measured reflection intensity, the blue region in the middle of the image, corresponds to the location of the SRRs patterned on the graphene, as the metasurface cancels out the reflection at its resonance wavelength where its impedance matches the impedance of incoming wave. After determining the location of the metasurface area through spatially resolved reflectance measurements, spectral measurements were carried out from the middle of this area, with applied gate voltage varied from –90V to 90V, and are shown in Fig. 2(c). The main reflection minimum corresponding to the resonance wavelength of the metasurface shifts from 5.05 µm when graphene is at its CNP ($V_g = 60$V) to 4.95 µm when $V_g = -90$V (note that the feature at 4.2 µm is due to the presence of CO_2).

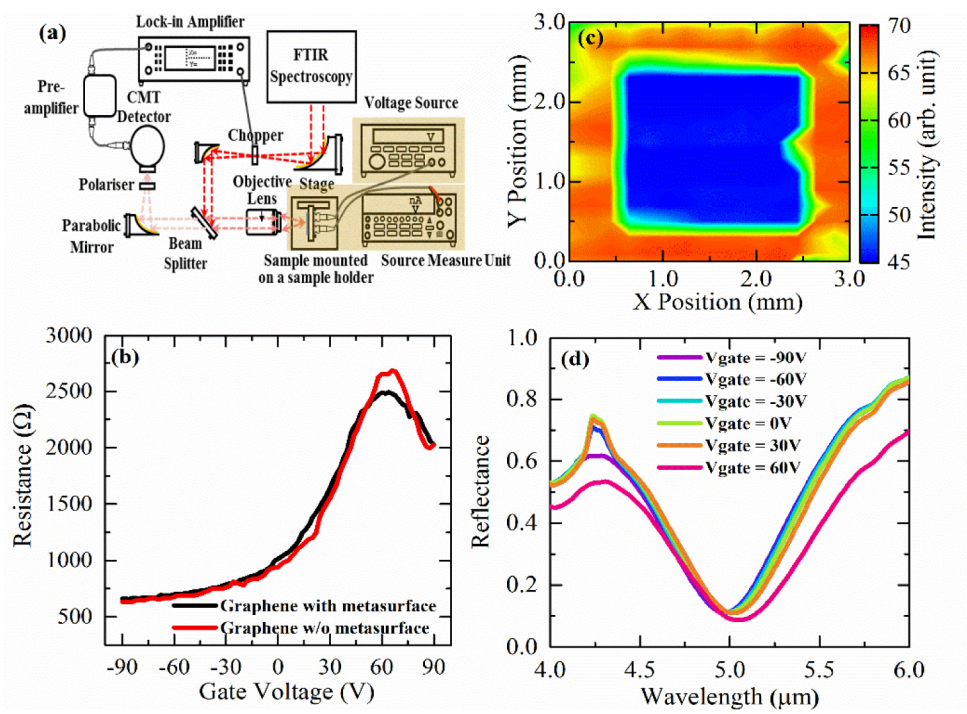

Fig. 2. (a) Schematic of the reflection intensity measurement setup to locate the position of the patterns. Once located, the stage moves to center of the pattern and optical chopper is removed from the setup for measuring the spectrum. Yellow shaded region was also utilized to measure the field effect characteristic of the device. (b) Field effect characteristic curves of graphene with metasurface patterned on the top and without metasurface on the top. (c) Spatially resolved broadband reflectance map from the graphene metasurface modulator (d) Measured reflection spectra of graphene metasurface modulator with gate voltage ranging from –90V to 60V (V_{CNP}).

Optics EXPRESS

3. Modelling and discussion

To explore the working mechanism of the graphene metasurface modulator, numerical simulations were performed using a commercial full wave simulation software, Lumerical FDTD solutions. Periodic boundary conditions were applied in the x- and y- directions as the metasurface patterned area is larger than the beam spot size, and perfect matching layer conditions were implemented on z-axis direction to simulate the open boundary condition. The geometric parameters of the structure were taken from electron microscopy images of the device, with a value of 1.35 for the relative refractive index of SiO_2 and the conductivities of Al and Au as 3.77×10^7 S/m and 4.1×10^7 S/m, respectively [32]. The monolayer CVD graphene used in this device is modelled as a conductive surface whose complex conductivity $\sigma(\omega, \mu_c, \tau, T)$ is defined by Kubo formula [33], in which ω is angular frequency, μ_c is Fermi level chemical potential, T represents the temperature, which in this case is the room temperature. The value of the relaxation time, τ, was taken as 50fs, consistent with the measurement of the carrier mobility in similar devices [29]. The Fermi level (E_F) of the graphene can be obtained from the applied gate voltage using the parallel plate capacitor model [25]:

$$\left|E_F\right| = \hbar v_F \sqrt{\frac{\pi \varepsilon_r \varepsilon_0 \left|V_g - V_{CNP}\right|}{e t_s}} \tag{1}$$

where $\hbar$ is the reduced Planck constant, $v_F = 1.1 \times 10^6$ m/s is the Fermi velocity, ε_r, t_s are the relative permittivity and thickness of the SiO_2 layer, and e, ε_0 are elementary charge and vacuum permittivity. With a charge neutral point of $V_{CNP} = 60$V, sweeping the gate voltage between −90V to 90V therefore varies the Fermi energy from 0eV to 0.288eV.

The simulated reflection spectra are plotted as the solid curves in Fig. 3(a) for different values of the Fermi energy. As clearly observed, the reflection minima shifts to a shorter wavelength when the carrier concentration in graphene is increased through gating. As shown in Fig. 3(b), where the wavelength at the minima is plotted as a function of gate voltage, there is good agreement with the experimental results. The slight differences between the simulation and experimental results are mainly due to the fact that in the experiment the incident light is not exactly a plane wave because of the use of a reflecting objective lens [34]. In addition, the extra contact pads and bonding wires on the device may also retransmit electromagnetic signal and therefore affects the resonance performance of the modulator. Following the method of Smith et al [35], we also extracted precise phase information by subtracting the additional propagation phase from the wave source to the device and the device to the monitor. As shown in Fig. 3(c), substantial phase modulation can be observed accompanied with the change on reflection amplitude when Fermi level increases. The phase modulation reaches a maximum of 150° when the Fermi level increases from 0eV to 0.4eV. Although we were only able to apply a maximum −90V gate voltage, which will just shift E_F to 0.288eV, previous results have shown that larger shifts of E_F can be can be achieved with higher gate voltages or thinner insulating layers. The field distribution was also investigated to see the interaction between the ring resonators and the graphene. As shown in Fig. 3(d), the electric field is highly confined in the gap both in xy plane (laterally) and along z-axis (vertically). Since this strong localized field overlaps with the graphene, this strong coupling can introduce a wide tuning range to the device.

Optics EXPRESS

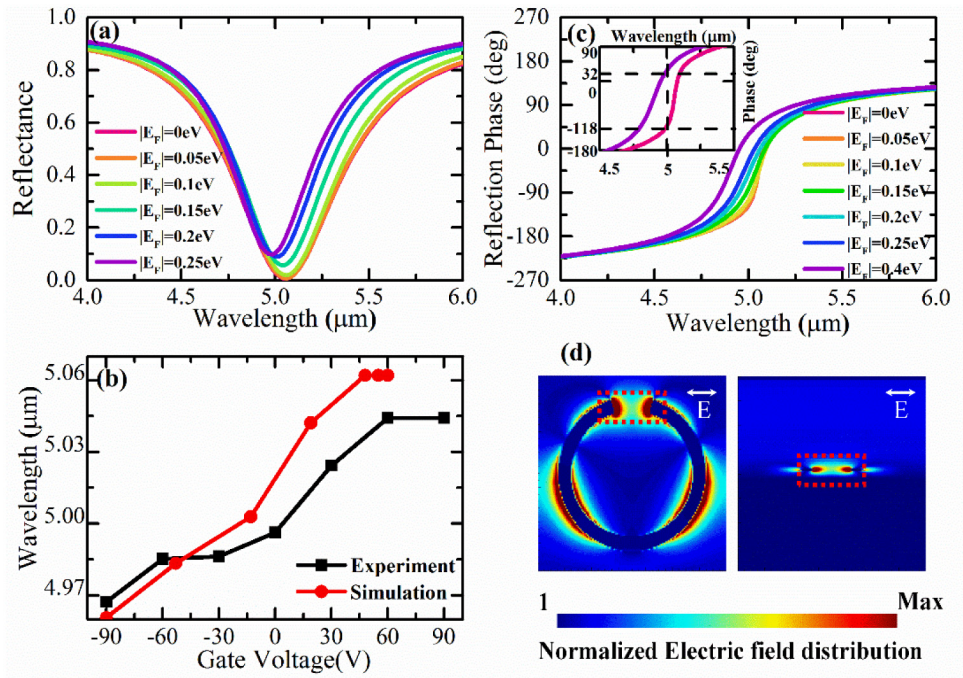

Fig. 3. (a) Simulated reflection spectra of modulator with Fermi level of graphene ranging from 0.25eV to 0eV (Dirac point). (b) Simulated and experimental resonant wavelength. For simulation curve, gate voltage is converted from Fermi level by Eq. (1). (c) Retrieved phase change due to the shift of Fermi level, inlet is a zoom into the axes in order to show the phase modulation achieved by the modulator at 5μm when Fermi level increases from 0eV to 0.4eV (d) cross sectional normalized electric field distribution at resonance wavelength in the x-y plane (left) and in the x-z plane intersecting the gap of SRRs (right)

4. Applications

Recent research has shown that such an active modulator is an ideal building block for reconfigurable metasurfaces, which have a wide range of applications such as radar [12], compact lenses [36,37], beam steering lenses [38,39], and dynamic holograms [13,40,41]. In this section, we demonstrate the feasibility of constructing a reconfigurable metasurface using the modulators described earlier. Simulation results show the capability of reflecting the reflective beam to an anomalous angle under normal incident plane wave at 5 μm when the graphene is electrostatically gated.

When waves propagate through a boundary between two different isotropic media, their refraction and reflection follow generalized Snell's law [42]

$$\sin(\theta_r) - \sin(\theta_i) = \frac{\lambda_0}{2\pi n_i}\frac{d\phi}{dx} \tag{2}$$

where θ_r is the reflection angle, θ_i is the angle of incidence, n_i is the refractive index of the material at incidence side, λ_0 is the wavelength of the incident wave, and $d\phi/dx$ is the gradient of phase discontinuity along the interface (x-axis direction). For normal cases, the interfaces are usually uniform so that there is no phase discontinuity along the surface ($d\phi/dx = 0$) and thus the reflection of wave follows conventional Snell's law. However, if a varying phase response is introduced to this interface, a nonlinear relation between θ_r and θ_i will occur. For normal incidence in air, the anomalous reflection angle θ_r, derived from Eq. (2), can be calculated as

Optics EXPRESS

$$\theta_r = \sin^{-1}\left(\frac{\lambda_0}{2\pi}\frac{d\phi}{dx}\right) \tag{3}$$

As the graphene metasurface modulator is capable of achieving a wide range of phase modulation, we specifically choose designs with four different geometric parameters as shown in Table 1. We aligned these four modulators into a 4 × 1 super lattice, as shown in Fig. 4(a). It should be noted that these four modulators are designed to have a linear spatial phase profile covering 0 to 2π in a super lattice when the Fermi level of graphene is 0.4eV and have nearly identical reflection phases when the Fermi level of graphene returns to the Dirac point. This enables dynamic beam steering using the applied gate voltage. At normal incidence, and with the gate voltage $V_g = V_{CNP}$, light will be reflected back at the normal to the surface as there is negligible phase discontinuity between every modulator. Applying a gate voltage such that E_F increases by 0.4eV, causes a π/2 phase increment between two adjacent modulators along x-axis direction to be introduced and the reflection angle changes from 0° to 29.6° (Eq. (3)). The calculated far-field scattering patterns of the lens, in polar coordinates, are plotted in Figs. 4(c) and 4(d), for zero and an applied bias respectively. The results clearly shows that a 45% steering efficiency can be achieved together with a 30° deflection angle, which in good agreement with the calculated reflection angle, 29.6°.

Table 1. Geometric Parameters of modulators used in beam steering lens

Modulator	r_1 (nm)	w (nm)	degree of gap θ (deg)	with or without graphene
1	900	120	20	Without
2	900	220	32	With
3	900	120	20	With
4	1120	70	66	With

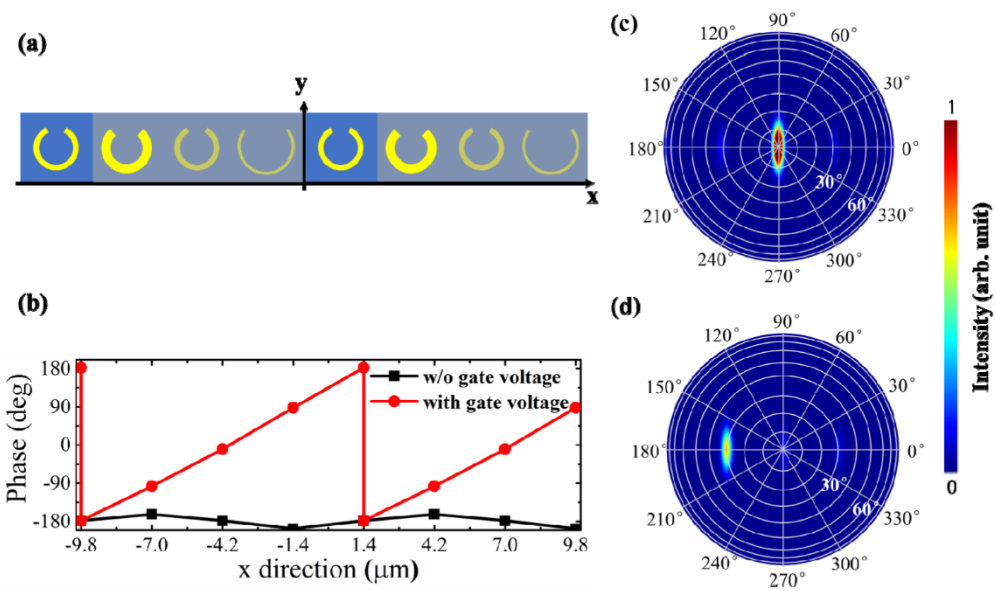

Fig. 4. (a) Schematic of two adjacent super lattices of beam steering modulator constructed by four modulators with different geometric parameters to achieve the necessary reflection phases. (b) The phase profile along x-axis for non-biased and biased lenses shown in (a). (c)&(d) Numerical simulations of scattering farfield pattern of non-biased (c) and biased lens (d), showing specular and anomalous reflection at λ = 5 μm respectively.

5. Conclusion

In conclusion, we have demonstrated a graphene based mid-infrared reflective modulator, where the wavelength at which the minimum in reflection occurs can be directly controlled by

Optics EXPRESS

an applied bias, with the size of the shift being in good agreement with the simulations. We also demonstrate the feasibility of creating a beam steering lens by constructing four such modulators but with different geometric parameters as a new super lattice. Simulations show that, as a 0 to 2π phase variation over the unit cell will be established as soon as a gate voltage is applied, the gated lens will reflect the beam with an extra 30 degrees compared to when the lens is unbiased.

Funding

Engineering and Physical Sciences Research Council (EPSRC) of the United Kingdom EP/L015331/1, EP/J018651/1, EP/S001557/1 and EP/P026656/1

Acknowledgment

C. S., I. J. L. and G. R. N. acknowledge financial support from the Engineering and Physical Sciences Research Council (EPSRC) of the United Kingdom via the Centre for Doctoral Training in Electromagnetic Metamaterials (No. EP/L015331/1). G. R. N. also acknowledges the support of EPSRC via a Fellowship in Frontier Manufacturing (No. EP/J018651/1) and I. J. L. acknowledges the EPSRC grants No. EP/S001557/1 and EP/P026656/1. Data published in this paper are available from the University of Exeter repository at https://doi.org/10.24378/exe.1304.

References

1. T. J. Yen, W. J. Padilla, N. Fang, D. C. Vier, D. R. Smith, J. B. Pendry, D. N. Basov, and X. Zhang, "Terahertz magnetic response from artificial materials," Science **303**(5663), 1494–1496 (2004).
2. C. L. Holloway, E. F. Kuester, J. A. Gordon, J. O'Hara, J. Booth, and D. R. Smith, "An overview of the theory and applications of metasurfaces: The two-dimensional equivalents of metamaterials," IEEE Antennas Propag. **54**(2), 10–35 (2012).
3. Q. Feng, M. Pu, C. Hu, and X. Luo, "Engineering the dispersion of metamaterial surface for broadband infrared absorption," Opt. Lett. **37**(11), 2133–2135 (2012).
4. Y. Fan, N. H. Shen, T. Koschny, and C. M. Soukoulis, "Tunable terahertz meta-surface with graphene cut-wires," ACS Photonics **2**(1), 151–156 (2015).
5. X. Ni, A. V. Kildishev, and V. M. Shalaev, "Metasurface holograms for visible light," Nat. Commun. **4**(1), 2807 (2013).
6. Z. Wei, Y. Cao, X. Su, Z. Gong, Y. Long, and H. Li, "Highly efficient beam steering with a transparent metasurface," Opt. Express **21**(9), 10739–10745 (2013).
7. Q. Wang, X. Zhang, Y. Xu, J. Gu, Y. Li, Z. Tian, R. Singh, S. Zhang, J. Han, and W. Zhang, "Broadband metasurface holograms: toward complete phase and amplitude engineering," Sci. Rep. **6**(1), 32867 (2016).
8. X. Wu, Y. Meng, L. Wang, J. Tian, S. Dai, and W. Wen, "Anisotropic metasurface with near-unity circular polarization conversion," Appl. Phys. Lett. **108**(18), 183502 (2016).
9. L. Zhu, F. Y. Meng, L. Dong, J. H. Fu, F. Zhang, and Q. Wu, "Polarization manipulation based on electromagnetically induced transparency-like (EIT-like) effect," Opt. Express **21**(26), 32099–32110 (2013).
10. H. T. Chen, W. J. Padilla, J. M. Zide, A. C. Gossard, A. J. Taylor, and R. D. Averitt, "Active terahertz metamaterial devices," Nature **444**(7119), 597–600 (2006).
11. M. Liu, X. Yin, E. Ulin-Avila, B. Geng, T. Zentgraf, L. Ju, F. Wang, and X. Zhang, "A graphene-based broadband optical modulator," Nature **474**(7349), 64–67 (2011).
12. T. J. Cui, M. Q. Qi, X. Wan, J. Zhao, and Q. Cheng, "Coding metamaterials, digital metamaterials and programmable metamaterials," Light Sci. Appl. **3**(10), e218 (2014).
13. L. Li, T. Jun Cui, W. Ji, S. Liu, J. Ding, X. Wan, Y. Bo Li, M. Jiang, C. W. Qiu, and S. Zhang, "Electromagnetic reprogrammable coding-metasurface holograms," Nat. Commun. **8**(1), 197 (2017).
14. L. Wang, L. Li, Y. Li, H. C. Zhang, and T. J. Cui, "Single-shot and single-sensor high/super-resolution microwave imaging based on metasurface," Sci. Rep. **6**(1), 26959 (2016).
15. A. R. Katko, A. M. Hawkes, J. P. Barrett, and S. A. Cummer, "RF limiter metamaterial using p-i-n diodes," IEEE Antennas Wirel. Propag. Lett. **10**, 1571–1574 (2011).
16. S. Savo, D. Shrekenhamer, and W. J. Padilla, "Liquid crystal metamaterial absorber spatial light modulator for THz applications," Adv. Opt. Mater. **2**(3), 275–279 (2014).
17. M. D. Goldflam, T. Driscoll, B. Chapler, O. Khatib, N. Marie Jokerst, S. Palit, D. R. Smith, B. J. Kim, G. Seo, H. T. Kim, M. D. Ventra, and D. N. Basov, "Reconfigurable gradient index using VO2 memory metamaterials," Appl. Phys. Lett. **99**(4), 044103 (2011).
18. A. Lyakh, R. Maulini, A. Tsekoun, R. Go, and C. K. N. Patel, "Intersubband absorption of quantum cascade laser structures and its application to laser modulation," Appl. Phys. Lett. **92**(21), 211108 (2008).

Optics EXPRESS

19. T. Roy, S. Zhang, I. W. Jung, M. Troccoli, F. Capasso, and D. Lopez, "Dynamic metasurface lens based on MEMS technology," APL Photonics **3**(2), 021302 (2018).
20. K. Bolotin, K. Sikes, Z. Jiang, M. Klima, G. Fudenberg, J. Hone, P. Kim, and H. Stormer, "Ultrahigh electron mobility in suspended graphene," Solid State Commun. **146**(9-10), 351–355 (2008).
21. K. S. Novoselov, V. I. Fal'ko, L. Colombo, P. R. Gellert, M. G. Schwab, and K. Kim, "A roadmap for graphene," Nature **490**(7419), 192–200 (2012).
22. A. K. Geim, "Graphene: status and prospects," Science **324**(5934), 1530–1534 (2009).
23. A. Andryieuski and A. V. Lavrinenko, "Graphene metamaterials based tunable terahertz absorber: effective surface conductivity approach," Opt. Express **21**(7), 9144–9155 (2013).
24. X. He, F. Liu, F. Lin, and W. Shi, "Graphene patterns supported terahertz tunable plasmon induced transparency," Opt. Express **26**(8), 9931–9944 (2018).
25. Y. Zhang, T. Li, Q. Chen, H. Zhang, J. F. O'Hara, E. Abele, A. J. Taylor, H. T. Chen, and A. K. Azad, "Independently tunable dual-band perfect absorber based on graphene at mid-infrared frequencies," Sci. Rep. **5**(1), 18463 (2015).
26. H. Huang, H. Xia, W. Xie, Z. Guo, H. Li, and D. Xie, "Design of broadband graphene-metamaterial absorbers for permittivity sensing at mid-infrared regions," Sci. Rep. **8**(1), 4183 (2018).
27. Y. Cai, J. Zhu, Q. H. Liu, T. Lin, J. Zhou, L. Ye, and Z. Cai, "Enhanced spatial near-infrared modulation of graphene-loaded perfect absorbers using plasmonic nanoslits," Opt. Express **23**(25), 32318–32328 (2015).
28. C. Sun, Z. Dong, J. Si, and X. Deng, "Independently tunable dual-band plasmonically induced transparency based on hybrid metal-graphene metamaterials at mid-infrared frequencies," Opt. Express **25**(2), 1242–1250 (2017).
29. P. Q. Liu, I. J. Luxmoore, S. A. Mikhailov, N. A. Savostianova, F. Valmorra, J. Faist, and G. R. Nash, "Highly tunable hybrid metamaterials employing split-ring resonators strongly coupled to graphene surface plasmons," Nat. Commun. **6**(1), 8969 (2015).
30. I. J. Luxmoore, C. H. Gan, P. Q. Liu, F. Valmorra, P. Li, J. Faist, and G. R. Nash, "Strong coupling in the far-infrared between graphene plasmons and the surface optical phonons of silicon dioxide," ACS Photonics **1**(11), 1151–1155 (2014).
31. C. Shi, N. H. Mahlmeister, I. J. Luxmoore, and G. R. Nash, "Metamaterial-based graphene thermal emitter," Nano Res. **11**(7), 3567–3573 (2018).
32. R. A. Serway and J. W. Jewett, Principles of physics (2nd Ed.). Fort Worth, TX: Saunders College Pub (1998).
33. G. W. Hanson, "Dyadic Green's Functions and Guided Surface Waves for a Surface Conductivity Model of Graphene," J. Appl. Phys. **103**(6), 064302 (2008).
34. S. Kim, M. S. Jang, V. W. Brar, Y. Tolstova, K. W. Mauser, and H. A. Atwater, "Electronically tunable extraordinary optical transmission in graphene plasmonic ribbons coupled to subwavelength metallic slit arrays," Nat. Commun. **7**(1), 12323 (2016).
35. D. R. Smith, S. Schultz, P. Markoš, and C. M. Soukoulis, "Determination of effective permittivity and permeability of metamaterials from reflection and transmission coefficients," Phys. Rev. B Condens. Matter Mater. Phys. **65**(19), 195104 (2002).
36. K. Chen, Y. Feng, F. Monticone, J. Zhao, B. Zhu, T. Jiang, L. Zhang, Y. Kim, X. Ding, S. Zhang, A. Alù, and C.-W. Qiu, "A reconfigurable active huygens' metalens,"," Adv. Mater. **29**(17), 1606422 (2017).
37. H. S. Ee and R. Agarwal, "Tunable metasurface and flat optical zoom lens on a stretchable substrate," Nano Lett. **16**(4), 2818–2823 (2016).
38. C. R. de Galarreta, A. M. Alexeev, Y. Y. Au, M. Lopez-Garcia, M. Klemm, M. Cryan, J. Bertolotti, and C. D. Wright, "Nonvolatile Reconfigurable Phase-Change Metadevices for Beam Steering in the Near Infrared," Adv. Funct. Mater. **28**(10), 1704993 (2018).
39. P. P. Iyer, M. Pendharkar, and J. A. Schuller, "Electrically reconfigurable metasurfaces using heterojunction resonators," Adv. Opt. Mater. **4**(10), 1582–1588 (2016).
40. Q. Wang, E. T. Rogers, B. Gholipour, C. M. Wang, G. Yuan, J. Teng, and N. I. Zheludev, "Optically reconfigurable metasurfaces and photonic devices based on phase change materials," Nat. Photonics **10**(1), 60–65 (2016).
41. Z. Zhu, P. G. Evans, R. F. Haglund, Jr., and J. G. Valentine, "Dynamically reconfigurable metadevice employing nanostructured phase-change materials," Nano Lett. **17**(8), 4881–4885 (2017).
42. N. Yu, P. Genevet, M. A. Kats, F. Aieta, J. P. Tetienne, F. Capasso, and Z. Gaburro, "Light propagation with phase discontinuities: generalized laws of reflection and refraction," Science **334**(6054), 333–337 (2011).

144.173.177.79 {ts '2019-05-14 08:53:21'}